

Photoinduced Valence Tautomerism of a Cobalt-Dioxolene Complex Revealed with Femtosecond M-edge XANES

Ryan Ash, Kaili Zhang, Josh Vura-Weis*

Department of Chemistry, University of Illinois at Urbana-Champaign

* Corresponding author: vuraweis@illinois.edu

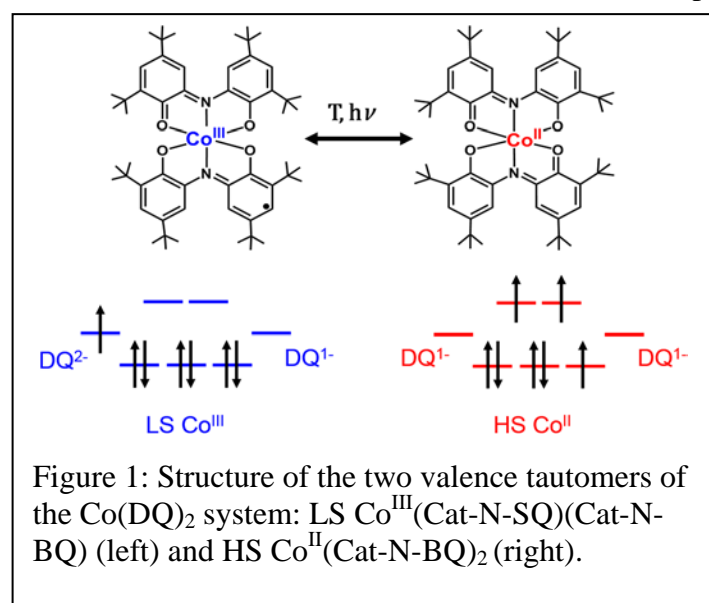
Abstract

Cobalt complexes that undergo charge-transfer induced spin-transitions (CTIST) or valence tautomerism (VT) from low spin (LS) Co^{III} to high spin (HS) Co^{II} are potential candidates for magneto-optical switches. We use $M_{2,3}$ -edge XANES spectroscopy with 40 fs time resolution to measure the excited-state dynamics of $\text{Co}^{\text{III}}(\text{Cat-N-SQ})(\text{Cat-N-BQ})$, where Cat-N-BQ and Cat-N-SQ are the singly and doubly reduced forms of the 2-(2-hydroxy-3,5-di-tert-butylphenyl-imino)-4,6-di-tert-butylcyclohexa-3,5-dienone ligand. The extreme ultraviolet probe pulses, produced using a tabletop high-harmonic generation light source, measure $3p \rightarrow 3d$ transitions and are sensitive to the spin and oxidation state of the Co center. Photoexcitation at 525 nm produces a low-spin Co^{II} ligand-to-metal charge transfer state which undergoes intersystem crossing to high-spin Co^{II} in 67 fs. Vibrational cooling from this hot HS Co^{II} state competes on the hundreds-of-fs timescale with back-intersystem crossing to the ground state, with 60% of the population trapped in a cold HS Co^{II} state for 24 ps. Ligand field multiplet simulations accurately reproduce the ground-state spectra and support the excited-state assignments. This work demonstrates the ability of $M_{2,3}$ -edge XANES to measure ultrafast photophysics of molecular Co complexes.

1. Introduction

Spin crossover (SCO) in transition metal complexes has gathered considerable attention for its potential use in magneto-optical switching and high-density data storage devices.¹⁻⁵ Molecules undergoing SCO exhibit changes in optical and magnetic properties with external stimuli such as temperature, pressure, or light. Upon initiation by a laser pulse, a cascade of coupled electronic and nuclear motion propels a molecular system from a low spin (LS) state into a metastable high spin (HS) state. Most SCO complexes have LS and HS states that only differ in the electron configuration on the metal center, but several cobalt complexes have LS and HS states with a change in the electronic configuration of both the metal and ligands. The difference between the states involves an electron transfer between metal and ligand orbitals, with the phenomenon referred to as a charge-transfer induced spin-transition (CTIST) or valence tautomerism (VT). This class of compounds includes well studied materials such as Co-Fe Prussian Blue analogues and Co dioxolene complexes.⁵⁻⁹ Dioxolene ligands have valence orbitals close in energy to those of third-row transition metal d orbitals, and can exist in multiple oxidation states. Previous results showed that the electronic structure of the two valence tautomers are localized, and can be thought of as electron transfer between the ligand and metal, with the metal center changing from LS $\text{Co}^{\text{III}} \leftrightarrow \text{HS Co}^{\text{II}}$.¹⁰⁻¹³

One such compound that exhibits valence tautomerism is $\text{Co}^{\text{III}}(\text{Cat-N-SQ})(\text{Cat-N-BQ})$, where Cat-N-BQ is the singly reduced 2-(2-hydroxy-3,5-di-tert-butylphenyl-imino)-4,6-di-tert-butylcyclohexa-3,5-dienone ligand and Cat-N-SQ is the doubly reduced analogue (Figure 1). This molecule interconverts between LS $\text{Co}^{\text{III}}(\text{Cat-N-SQ})(\text{Cat-N-BQ})$ and HS $\text{Co}^{\text{II}}(\text{Cat-N-BQ})_2$.^{10,14} The LS tautomer is a spin doublet with a radical localized on a single (Cat-N-SQ) ligand, whereas the HS tautomer is a spin quartet with the spin localized on the metal center. For the sake of brevity, both tautomers will be referred to as $\text{Co}(\text{DQ})_2$, where DQ is a singly or doubly reduced Schiff-base diquinone ligand. Ultrafast optical and infrared transient absorption studies with 200 fs time resolution have shown that upon photoexciting the LS tautomer at 525



nm, the HS state forms in hundreds of femtoseconds.^{15,16} An intermediate state was identified in the optical transient absorption (OTA) results with a lifetime of ≤ 180 fs (potentially limited by the instrument response function), which was suggested to be a LS Co^{II} / oxidized ligand state. However, the multitude of intraligand transitions in the visible region makes assignment of the electronic structure of the Co center difficult. Recent calculations by van Veenendaal of a single Co^{II} atom coupled to a symmetric M-CN vibrational mode suggested that intersystem crossing (ISC) from the Frank-Condon LS Co^{II} state to the metastable HS state could occur within 20 fs, and the Co center might populate higher energy quartet states during relaxation.¹⁷

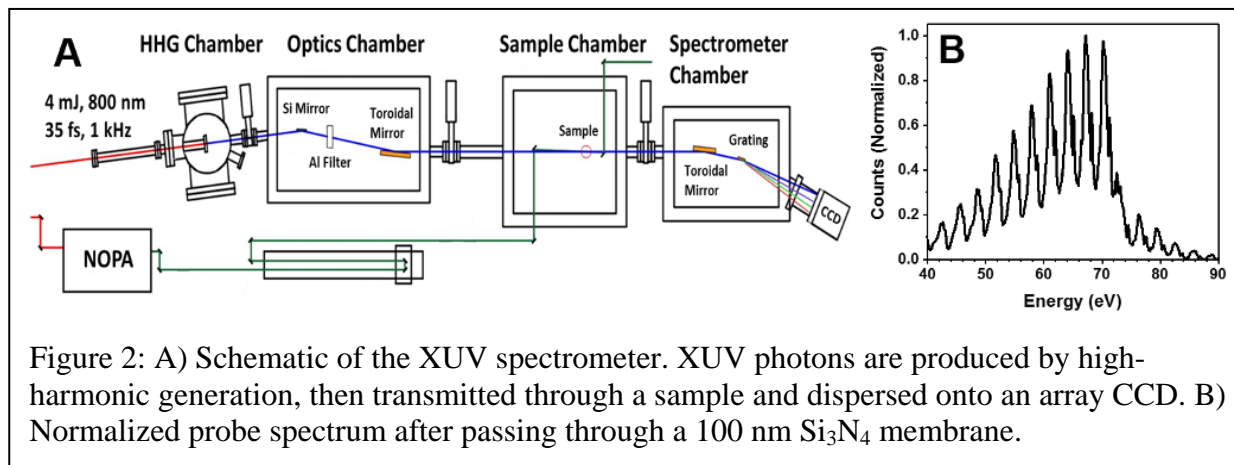
Despite the great interest in Co^{II} systems undergoing CTIST/VT, no transient experiments have been performed that directly probe the electronic state of the metal center with the time resolution necessary to observe the intersystem crossing. Many commonly used techniques to characterize metal-centered spin states, such as magnetometry and EPR, lack the femtosecond time resolution necessary to observe short lived excited states. Core-level techniques such as L-edge X-ray absorption near-edge structure (XANES) and $\text{K}\beta$ x-ray fluorescence are sensitive to the spin of the Co center^{18,19} and have been successfully used to probe the temperature-dependent spin state of a valence tautomer similar to the one studied here.¹¹ While ultrafast core-level spectroscopy of Fe complexes has provided important insights into the excited-state electronic structure of molecules such as Fe^{II} polypyridyl complexes,^{20–24} femtosecond experiments at the Co edge are less common.^{25–28} The intermediate spin states involved in photoinduced VT have therefore remained elusive.

Extreme ultraviolet (XUV) spectroscopy probes the $\text{M}_{2,3}$ -edge of third-row transition metals (hereafter written as “M-edge” for brevity). The $3\text{p} \rightarrow 3\text{d}$ dipole-allowed transitions lying between 30-100 eV contain information about the oxidation state, spin state, and coordination geometry of the metal center, and can be predictably reproduced using ligand-field multiplet (LFM) simulations.^{29–32} The development of ultrafast XUV light sources based on high-harmonic generation (HHG) has extended the applicability of M-edge spectroscopy to study the dynamics of 3d transition metal complexes. Femtosecond M-edge XANES has been used to measure excited-state relaxation dynamics in Fe and Ni complexes^{31,33,34} and in transition metal oxide semiconductors,^{35–39} but its applicability to molecular cobalt complexes has not yet been demonstrated. In the present work, we use this emerging technique to measure the mechanism and timescale of ultrafast valence tautomerism in $\text{Co}(\text{DQ})_2$ from the perspective of the metal center, revealing an initial LS Co^{II} state that precedes competitive vibrational cooling and intersystem crossing processes.

2. Methods

$\text{Co}(\text{DQ})_2$ was synthesized according to literature procedures,¹⁰ and samples were deposited as ~125 nm thick films on 100 nm Si_3N_4 membranes via vacuum sublimation. The sublimation was performed at 1×10^{-5} torr and 210°C , with a deposition rate of 0.1-0.3 Å/s. The complex initially deposits as a mixture of the two valence tautomers, so films were then annealed at 170°C for 30 minutes to convert the majority of the film to the $^1\text{Co}^{\text{III}}(\text{Cat-N-SQ})(\text{Cat-N-BQ})$ phase.

XUV photons for M-edge XANES studies were produced via high-harmonic-generation using the instrument shown in Figure 2A. XUV pulses with a duration of ~15 fs are generated by focusing a Ti:sapphire driving laser pulse (800 nm, 4 mJ, 35 fs, 1 kHz) into a semi-infinite gas cell⁴⁰ containing 100 torr Ne. The residual 800 nm photons are attenuated with a Si mirror and 100 nm Al filter. The XUV pulse is then transmitted through the sample and dispersed onto an array CCD. As shown in Figure 2B, the broadband probe spans 40 to 90 eV. Odd harmonics of the 800 nm driving field create peaks every 3.1 eV,⁴¹ but the broad continuum beneath these peaks is suitable for absorption spectroscopy. The spectrometer resolution of roughly 0.3 eV is measured daily by fitting atomic transitions of Xe^+ and Kr^+ . The instrument is maintained at a pressure of $<10^{-6}$ torr to prevent absorption of the XUV probe by air. For transient absorption experiments, a fraction of the Ti:sapphire output (0.7 mJ) is fed into a noncollinear optical parametric amplifier (TOPAS White) to generate 10 μJ , 30 fs pulses centered at 525 nm. This



pump fluence generates an excitation fraction of ~14%, calculated using the measured absorbance at the pump wavelength. Samples are cooled by a stream of N₂ gas to reduce the effects of accumulative pump laser heating between shots. Time-zero and the instrument response function (IRF) of 40 fs FWHM were measured by concurrent transient absorption of the IRF-limited LMCT state in α -Fe₂O₃⁴².

M-edge spectra of transition metal complexes are simulated using ligand field multiplet (LFM) theory.^{29,30,32} Briefly, the metal center is modeled using a parametric Hamiltonian containing electron-nuclear and electron-electron coulomb terms, spin-orbit coupling and an electrostatic crystal field. Slater-Condon electron-electron repulsion and mixing parameters were reduced to 60-100% of their free ion values to account for electron delocalization. The simulation assumes an octahedral crystal field with the field splitting parameter 10Dq of 2.7 eV for LS Co^{III} and 1.5 eV for HS Co^{II}. The crystal field splitting for the LS Co^{II} simulation is also set to 2.7 eV to account for its preparation in a Frank-Condon state with the same ligand field as the LS Co^{III} state. Spin-orbit coupling constants were kept the same as the free ion values. A similar computational framework has been used successfully to understand L-edge spectra, including ultrafast studies of Fe^{II} spin crossover complexes.²⁴ Further information about the LFM simulations can be found in the Supporting Information section S2.

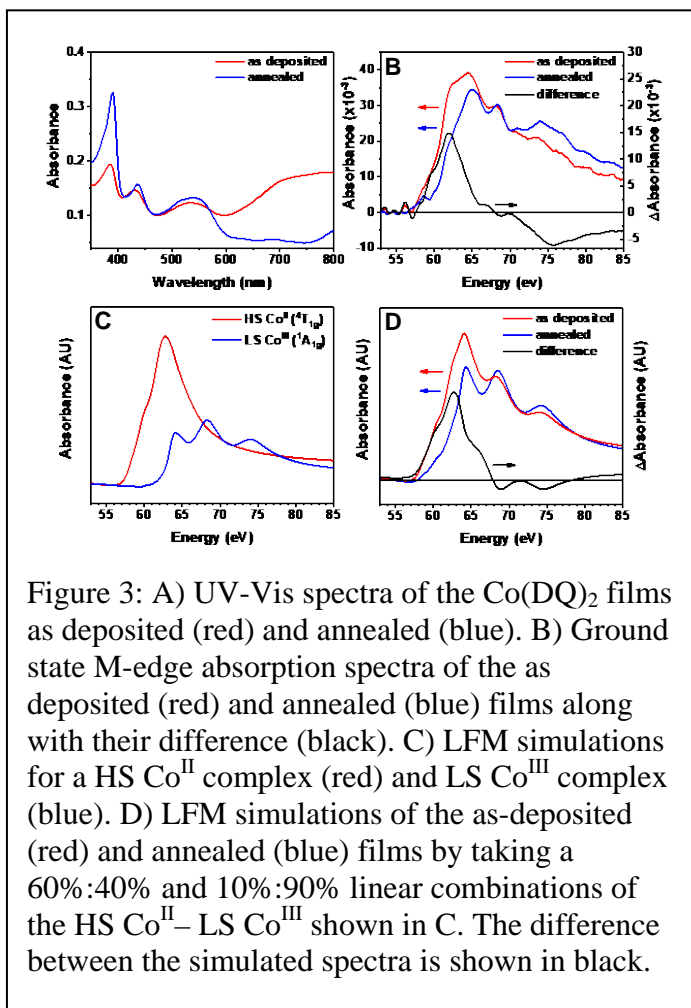
3. Results

3.1. Sample preparation and ground state spectra

Thermal evaporation of Co(DQ)₂ produces a film that is a mixture of the low-temperature LS Co^{III} and high-temperature HS Co^{II} tautomers. As shown in Figure 3A, the UV-Vis absorption spectrum of the as-deposited film has peaks at 390, 430 and 530 nm, in addition to a broad absorption feature from 700-800 nm. This low-energy absorption feature is assigned to the HS Co^{II} tautomer¹⁴. Upon annealing, the 700-800 nm feature disappears and the peaks at 390, 430 and 530 nm rise, indicating conversion from the HS Co^{II} tautomer to the LS Co^{III} tautomer. The annealing process removes the ability of Co(DQ)₂ to undergo thermally induced VT, with the film decomposing upon further heating before showing any spectral changes. The film can be redissolved in toluene, showing the same UV-Vis spectra as the synthesized compound and re-exhibiting thermal VT in solution upon heating above room temperature. The bulk solid does not exhibit the same behavior on annealing. The loss of thermal VT on annealing

is likely from a change in the molecular packing of the annealed film that increases the energy difference between the two valence tautomers.

Ground state M-edge XANES spectra of the as-deposited and annealed films are shown in Figure 3B. The annealed film has peaks at 65.0, 68.4, and 74.0 eV with a weak shoulder at 61.6 eV. In the as-deposited film, the 74.0 eV peak is attenuated and the 61.6 eV shoulder and main peak gain intensity, with the main peak shifting from 65.0 to 64.4 eV. The difference spectrum ($A_{\text{as-deposited}} - A_{\text{annealed}}$) in Figure 3A highlights the changes upon annealing, with a main peak at 62.1 eV, shoulders at 59.9 and 66.4 eV, and a broad negative feature from 70-85 eV. Two independent effects combine to blueshift the LS Co^{III} spectrum relative to HS Co^{II} . First, the increased effective nuclear charge on LS Co^{III} stabilizes the 3p orbitals. As in K-edge and L-edge XANES, an oxidation state change of +1 causes a 1-2 eV blueshift. Second, in the HS Co^{II} state there is increased exchange stabilization of the $3p^5 3d^6$ core-state, which redshifts high-spin spectra relative to their low-spin analogues²⁹. This behavior is also observed in $L_{2,3}$ -edge spectra of 3rd row transition metal complexes^{24,43}. The experimental spectral changes are in good agreement with LFM simulations of a combination of HS Co^{II} and LS Co^{III} species. As shown in Figure 3C, the LFM simulation for the HS Co^{II} species ($^4T_{1g}$) predicts a shoulder at 60.0 eV followed by a larger main peak at 63.0 eV. Note that we use Mulliken term symbols to denote the multiplicity and symmetry of the metal center, not the overall complex. The LS Co^{III} simulation ($^1A_{1g}$, with a radical on the ligand) predicts three features of similar intensity at 64.3, 68.7 and 74.3 eV. These peaks can be understood through a straightforward application of ligand field theory, as described in detail in the Supporting Information section S2. By forming linear combinations of the simulations and comparing them to the experimental spectra, we estimate the as-deposited film to be a mixture of a 60% HS Co^{II} : 40% LS Co^{III} . When annealed, we estimate this percentage shifts to 10%:90% (Figure 3D). Conveniently, the difference between the experimental annealed and as-deposited spectra gives the expected transient spectrum for photoinduced VT in the $\text{Co}(\text{DQ})_2$ system, with shoulders at 59.7 and 65.6 eV, main peak at 62.0 eV, and bleaches at 68.9 and 74.6 eV.



3.2. Transient M-edge XANES

Transient M-edge XANES spectra of $\text{Co}(\text{DQ})_2$ after photoexcitation at 525 nm are summarized as a contour plot in Figure 4A, showing the difference in absorption after laser pumping ($A_{\text{pump on}} - A_{\text{pump off}}$) as a function of energy and delay time between the pump and probe pulses. As noted in the methods section, absolute t_0 and the instrument response of 40 fs FWHM are measured by fitting the rise of the LMCT state in $\alpha\text{-Fe}_2\text{O}_3$. Spectral slices at several delay times are shown in Figure 4B. The IRF limited spectrum depicted in the 10 fs slice has a weak induced absorption at 61.5 eV and a bleach and from 72-80 eV. In the first 100 fs, the induced absorption feature rises and blueshifts to 62.5 eV. The dark blue line in Figure 4A tracks the energy of the peak maximum at each timepoint, and shows that this blueshift is complete by 60 fs. By 250 fs, the transient spectrum is similar to the difference spectrum between the as-deposited and annealed films, as expected for conversion of LS Co^{III} to HS Co^{II} . The difference between the spectrum after 250 fs and the as-deposited vs annealed spectrum is likely due either to a difference in the local environment (molecular packing) or to the photoexcited molecules not being fully vibrationally equilibrated.⁴⁴

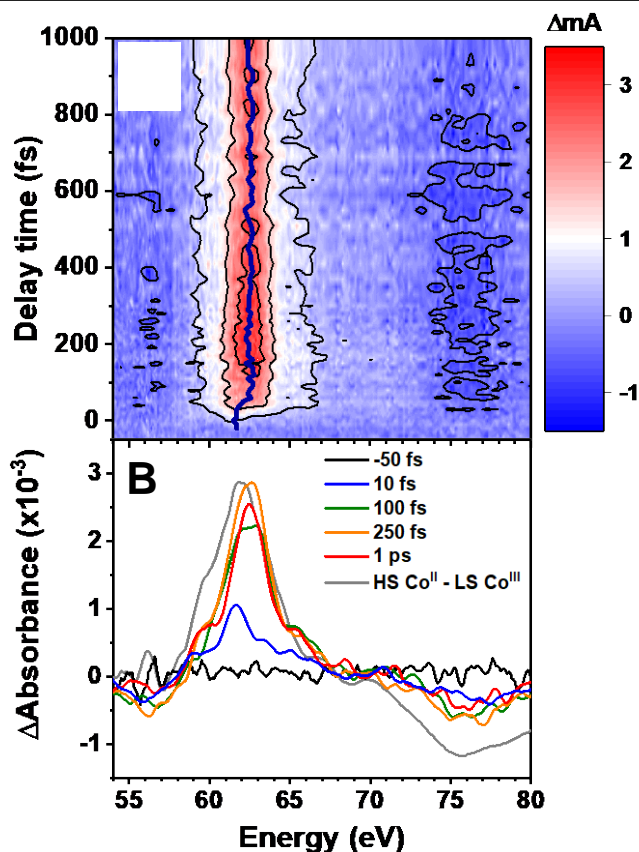
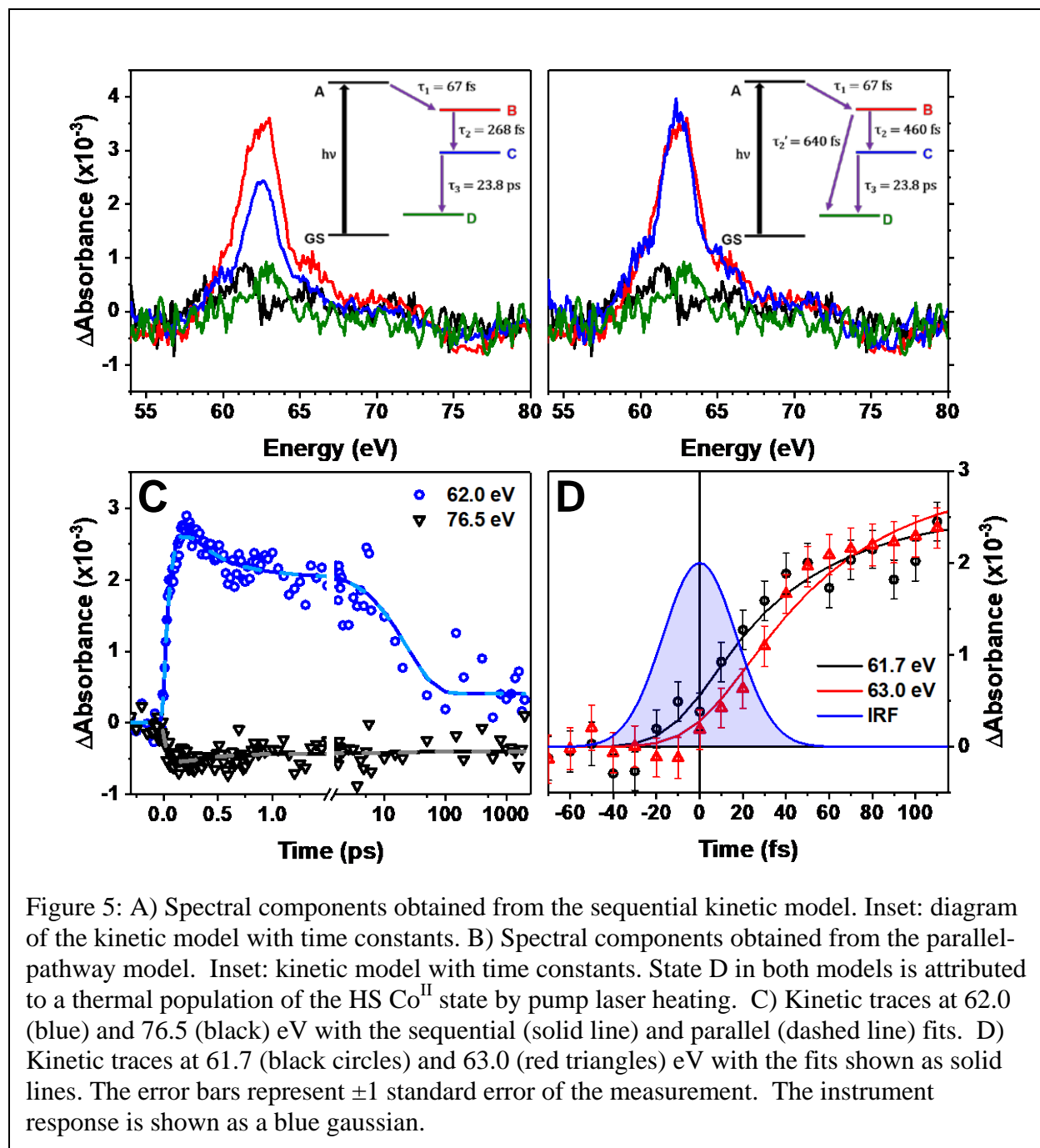


Figure 4: A) Contour plot of transient M-edge XANES of $\text{Co}(\text{DQ})_2$, with the dark blue trace showing the energy of the max induced absorption over time. B) Spectral slices within the first picosecond of laser excitation, showing a delayed rise of a feature that shifts to higher energies then reduces in intensity after a few hundred femtoseconds. The transient spectrum at 250 fs and beyond is similar in shape to the difference spectrum between annealed and unannealed films shown in gray, scaled to match the height of the 250 fs spectrum.

Within the first few ps, the transient signal drops by ~40% of the maximum observed value (Figure 5C), then decays further over the next 100 ps. A weak signal with a peak at 63.0 eV lasts longer than the time window of the experiment (> 2 ns). This long-time signal strongly resembles the GS difference spectrum. Based on the spectral shape and previous transient experiments using thin film samples,^{31,45} we assign the long-lived state as a thermal population of the Co^{II} HS state from pump laser heating. This heat shifts the equilibrium between the HS and LS isomers in the laser spot and temporarily results in a higher concentration of HS species. The spot cools before the next laser shot 1 ms later and restores the original equilibrium.

3.3. Kinetic modeling

The data was first fit to a 4-state $A \xrightarrow{k_1} B \xrightarrow{k_2} C \xrightarrow{k_3} D$ sequential model in which state D accounts for the persistent long-lived heat signal and not to a separate electronic state of the photoexcited molecules. Time zero and the 40 fs instrument response function are fixed to the values obtained from concurrent transient absorption of α -Fe₂O₃. Global fitting extracts 3 component spectra with time constants ($\tau = 1/k$) $\tau_1 = 67 \pm 3$ fs, $\tau_2 = 268 \pm 16$ fs, and $\tau_3 = 23.8 \pm 2.1$ ps. Component D is treated as a shelf with an infinite time constant as it does not decay over the 2 nanosecond experimental window. This kinetic model is summarized in the inset to Figure 5A. The IRF-limited first absorption feature (state A) has weak peaks centered at 61.7, 65.5 and 71.5 eV. The second and third component spectra (states B and C) are almost identical in shape having a main peak at 62.5 eV and shoulders at 60.0 and 65.2 eV, with the main difference being their intensities (Figure 5A). Specifically, state C has 40% lower intensity than state B. The fourth component spectrum (state D) has a similar shape as both B and C but is further reduced in intensity.



The similarity between the spectra of states B and C in the sequential model suggests that instead of the system passing through 3 different electronic states, there is another relaxation pathway from state B in the first few ps that results in a reduction in its population. Following this logic, the data was refit to a model with parallel relaxation pathways, as shown in the inset to Figure 5B. State B is assumed to be a vibrationally hot state that either cools to state C or relaxes directly to D. State C then relaxes slowly to state D. The extracted spectral components look almost identical to the sequential model fit with changes in scaling of state C. This parallel-model fit yields relaxation rates of $\tau_2 = 460 \pm 38$ fs for B \rightarrow C vibrational cooling and $\tau_2' = 640 \pm 19$ fs for B \rightarrow D relaxation to the ground state, with the same rate constants for τ_1 and τ_3 as in the

sequential model. The addition of these time constants closely matches τ_2 in the sequential model: $(1/\tau_2 + 1/\tau_2')^{-1} = 268$ fs. This parallel fit suggests that 40% of the overall population of the vibrationally hot state B relaxes to state D before vibrational cooling, which correlates well with the ~40% reduction in signal intensity between states B and C in the sequential model.

Both models give an identical fit to the data, with reconstructed kinetics compared to the data in Figure 5C. At early times, both models clearly capture an initial IRF-limited species A that evolves into a second species B in 67 fs. The time delay between these states is shown in Figure 5D, which plots the rise of the signal at 61.7 eV (the peak of A) and 63.0 eV (slightly to the blue of the peak of B). The rise at 63.0 is delayed by ~12 fs from the IRF-limited rise at 61.7 eV.

3.4. Assignment of component spectra

As discussed above, the global fit (or simple inspection of the early-time transient spectra) identifies two distinct states in the first tens of femtoseconds after photoexcitation. The spectra of these states A and B are reproduced in Figure 6A, and are assigned as low-spin and high-spin Co^{II} using the ligand field multiplet simulations shown in Figure 6B.

The LS Co^{II} (2E_g) simulation has three weak absorption features centered at 61.9, 66.5 and 71.2 eV, while the HS Co^{II} (${}^4T_{1g}$) simulation has a main peak at 62.5 eV with shoulders at 60.0 and 65.6 eV. The simulated LS Co^{II} spectrum matches the component spectrum for state A well both in shape and in its weak intensity compared to the HS Co^{II} spectrum. Similarly, the peak positions and overall shape of the HS Co^{II} simulation are good matches for the experimental state B, with the main difference being the height of the shoulders and the depth of the bleach past 66 eV. As was shown in Figure 4B, experimental states C and D are identical in shape to B within the noise level of the experiment. In conjunction with the parallel kinetic model in the previous section, state C is assigned as the vibrationally cold HS Co^{II} state, which to our metal-centered probe is not distinguishable from the hot HS Co^{II} state. As was discussed in Section 3.2, state D represents excess heat within the pump spot of the thin-film sample which shifts the HS/LS equilibrium and produces a long-lived excess of HS Co^{II} valence tautomers. Finally, we note that Gentili et al⁴⁶ proposed that the initial excitation could form a LS Co^{IV} species. We address this possibility in the Supporting Information section S3.

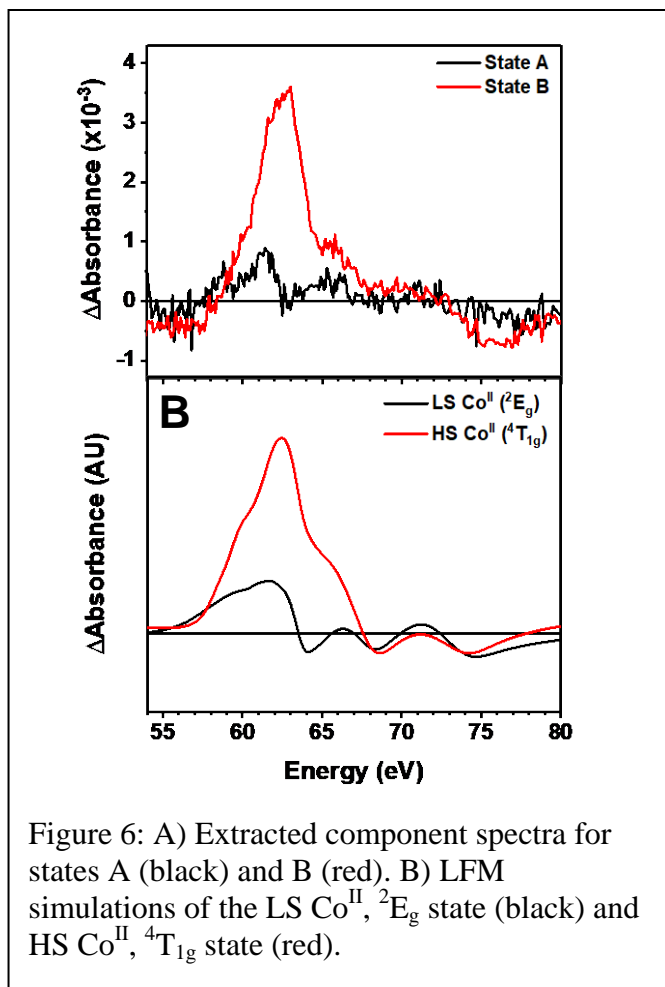
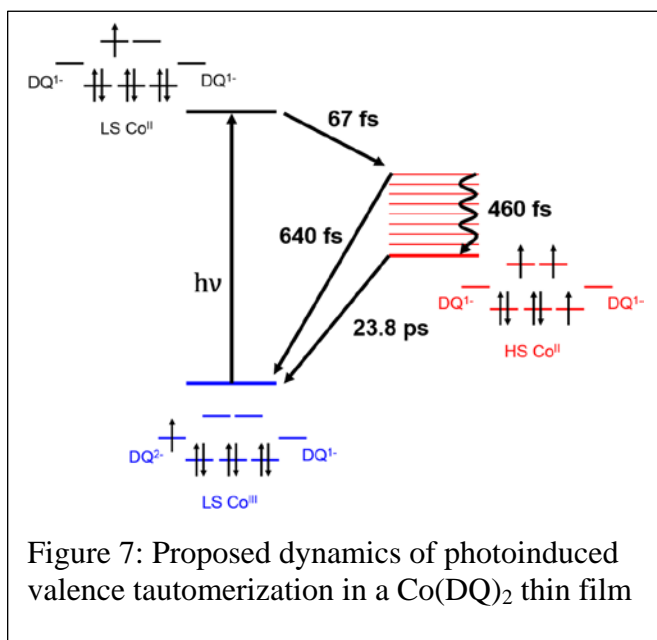


Figure 6: A) Extracted component spectra for states A (black) and B (red). B) LFM simulations of the LS Co^{II} , 2E_g state (black) and HS Co^{II} , ${}^4T_{1g}$ state (red).

4. Discussion

The photophysics described above are summarized in Figure 7. 525 nm excitation from the LS Co^{III} ground state forms an LMCT state with LS Co^{II} and an oxidized DQ¹⁻ ligand. The fast time resolution and spin state specificity of the XUV probe provides the first conclusive identification of the LS Co^{II} excited state. Intersystem crossing in 67 fs forms vibrationally hot HS Co^{II}. Back-ISC in 640 fs competes with a 460 fs vibrational cooling time that traps molecules in a cold HS Co^{II} state. From there, back-ISC occurs in 23.8 ps. A similar interplay between intersystem crossing and vibrational cooling has been observed in other transition metal complexes.⁴⁷ For example, photoexcitation of Cr(acac)₃ leads rapidly to an equilibrium between hot ⁴T₂ and ²E states via thermally activated intersystem crossing.⁴⁸⁻⁵¹ Approximately 20% of the population traps in a cold ²E state which relaxes in hundreds of ps. An important difference between the Cr(acac)₃ and Co(DQ)₂ systems should be noted: in Cr(acac)₃ the thermally activated back-ISC repopulates an excited state (⁴T₂), but in Co(DQ)₂ the ground state is repopulated.



Co(DQ)₂ was previously studied by optical transient absorption with ~200 fs time resolution.¹⁵ A time constant of 180 ± 20 fs was reported for the first relaxation step, which we have identified here as LS Co^{II} → HS Co^{II} intersystem crossing. This time constant was likely limited by the IRF or by a slight dependence of the optical signal on the ligand dynamics, and is therefore consistent with the M-edge XANES result. More significantly, the back-ISC lifetime from the cold HS Co^{II} state measured as 410 ps in chloroform solution is significantly slower than the 23.8 ps we measure in a thin film with M-edge XANES. This difference in relaxation times is likely a mixture of solvation and thin-film heating effects. Faster relaxation

from the HS Co^{II} state of a similar Co complex has been observed previously in doped polymer films and was attributed to an environment-dependent energy difference between the two tautomers.⁵² It is well known that solvation effects play a key role in the valence tautomerization process, and can either change the transition temperature or entirely deactivate the process.^{9,53-56} This has been attributed to intermolecular factors such as a change in polarity or lattice softness in crystalline VT compounds, which either changes the barrier or the energy difference between the two tautomers. It is likely that annealing produces one or both effects. The loss of thermal VT in the film suggests a stabilization of the LS Co^{III} tautomer, which lowers the activation barrier for back-ISC. This correlation between energy gap and relaxation time is well known in Fe^{II} systems, and is referred to as the inverse energy gap law.⁵⁷ Sample heating also contributes to fast back-ISC in the thin film. As shown in the Supporting Information section S1, optical transient absorption (OTA) data was collected on the same thin film sample used for XUV data collection and gave a 60 ps decay time. The difference in the relaxation times between the OTA

and M-edge experiments is likely due to the change from atmospheric convective cooling to cooling by a stream of N₂ in vacuum: the steady-state temperature of the sample is likely higher in the latter, which accelerates the thermally activated back-ISC. The development of in-vacuum thin liquid sheet-jets may soon allow transient XUV spectroscopy to be performed in the solution phase,^{58,59} allowing this environment dependence to be tested experimentally.

5. Conclusion

In summary, femtosecond XUV transient absorption spectroscopy shows that 525 nm excitation of the valence tautomeric complex Co(DQ)₂ forms a low-spin Co^{II} LMCT state within the 40 fs instrument response. The complex then undergoes rapid intersystem crossing in 67 fs to a hot high-spin Co^{II} state. Vibrational cooling in 460 fs competes with rapid back-intersystem crossing, with 40% of the excited-state population relaxing to the LS Co^{III} ground state from the hot HS Co^{II} state. The cold HS Co^{II} state relaxes the ground state in 24 ps, with a strong influence from sample temperature and environment. This work showcases the growing importance of ultrafast core-level spectroscopy for transition metal photophysics. The spin sensitivity of M-edge XANES revealed branching between vibrational and electronic relaxation that was not separable with visible-light probes. The fast time resolution and in-lab convenience of this technique makes it a promising complement to hard X-ray probes of Co complexes.

Supplementary Material

Optical transient absorption in thin films and in solution, ligand field multiplet simulations and assignment of spectra, IRF and time-zero determination, description of fit algorithm.

Acknowledgements

This material is based upon work supported by the National Science Foundation under Grant No. 1555245. The transient XUV instrument, including the nonlinear optical parametric amplifier, was built with funding from the Air Force Office of Scientific Research under AFOSR Award No. FA9550-14-1-0314. We thank Gregory S. Girolami for helpful discussions.

References:

- ¹ K. Senthil Kumar and M. Ruben, *Coord. Chem. Rev.* **346**, 176 (2017).
- ² P. Gutlich, *Coord. Chem. Rev.* **219–221**, 839 (2001).
- ³ O. Kahn and C.J. Martinez, *Science* **279**, 44 (1998).
- ⁴ M. Verdaguer, *Science* **272**, 698 (1996).
- ⁵ O. Sato, T. Iyoda, A. Fujishima, and K. Hashimoto, *Science* **272**, 704 (1996).
- ⁶ Y. Moritomo, H. Kamioka, T. Shibata, S. Nozawa, T. Sato, and S.I. Adachi, *J. Phys. Soc. Japan* **82**, 1 (2013).
- ⁷ D.N. Hendrickson and C.G. Pierpont, in *Spin Crossover Transit. Met. Compd. II* (2004), pp. 63–95.

- ⁸ O. Sato, A. Cui, R. Matsuda, J. Tao, and S. Hayami, *Acc. Chem. Res.* **40**, 361 (2007).
- ⁹ M. Slota, M. Blankenhorn, E. Heintze, M. Vu, R. Hübner, and L. Bogani, *Faraday Discuss.* **185**, 347 (2015).
- ¹⁰ S.K. Larsen and C.G. Pierpont, *J. Am. Chem. Soc.* **110**, 1827 (1988).
- ¹¹ H.W. Liang, T. Kroll, D. Nordlund, T.C. Weng, D. Sokaras, C.G. Pierpont, and K.J. Gaffney, *Inorg. Chem.* **56**, 737 (2017).
- ¹² D.M. Adams, L. Noodleman, and D.N. Hendrickson, *Inorg. Chem.* **36**, 3966 (1997).
- ¹³ O. Cador, F. Chabre, A. Dei, C. Sangregorio, J. Van Slageren, and M.G.F. Vaz, *Inorg. Chem.* **42**, 6432 (2003).
- ¹⁴ A. Caneschi, A. Cornia, and A. Dei, *Inorg. Chem.* **37**, 3419 (1998).
- ¹⁵ P.L. Gentili, L. Bussotti, R. Righini, A. Beni, L. Bogani, and A. Dei, *Chem. Phys.* **314**, 9 (2005).
- ¹⁶ N. Azzaroli, A. Lapini, M. Di Donato, A. Dei, and R. Righini, *J. Phys. Chem. B* **117**, 15492 (2013).
- ¹⁷ M. Van Veenendaal, *Sci. Rep.* **7**, 1 (2017).
- ¹⁸ J. Herrero-Martín, J.L. García-Muñoz, K. Kvashnina, E. Gallo, G. Subías, J.A. Alonso, and A.J. Barón-González, *Phys. Rev. B - Condens. Matter Mater. Phys.* **86**, 125106 (2012).
- ¹⁹ L.C. Wu, T.C. Weng, I.J. Hsu, Y.H. Liu, G.H. Lee, J.F. Lee, and Y. Wang, *Inorg. Chem.* **52**, 11023 (2013).
- ²⁰ W. Zhang, R. Alonso-Mori, U. Bergmann, C. Bressler, M. Chollet, A. Galler, W. Gawelda, R.G. Hadt, R.W. Hartsock, T. Kroll, K.S. Kjær, K. Kubiček, H.T. Lemke, H.W. Liang, D.A. Meyer, M.M. Nielsen, C. Purser, J.S. Robinson, E.I. Solomon, Z. Sun, D. Sokaras, T.B. van Driel, G. Vankó, T.-C. Weng, D. Zhu, and K.J. Gaffney, *Nature* **509**, 345 (2014).
- ²¹ H.T. Lemke, K.S. Kjær, R. Hartsock, T.B. Van Driel, M. Chollet, J.M. Glowina, S. Song, D. Zhu, E. Pace, S.F. Matar, M.M. Nielsen, M. Benfatto, K.J. Gaffney, E. Collet, and M. Cammarata, *Nat. Commun.* **8**, 15342 (2017).
- ²² P. Wernet, K. Kunnus, I. Josefsson, I. Rajkovic, W. Quevedo, M. Beye, S. Schreck, S. Grübel, M. Scholz, D. Nordlund, W. Zhang, R.W. Hartsock, W.F. Schlotter, J.J. Turner, B. Kennedy, F. Hennies, F.M.F. de Groot, K.J. Gaffney, S. Techert, M. Odelius, and A. Föhlisch, *Nature* **520**, 78 (2015).
- ²³ R.M. Jay, J. Norell, S. Eckert, M. Hantschmann, M. Beye, B. Kennedy, W. Quevedo, W.F. Schlotter, G.L. Dakovski, M.P. Minitti, M.C. Hoffmann, A. Mitra, S.P. Moeller, D. Nordlund, W. Zhang, H.W. Liang, K. Kunnus, K. Kubiček, S.A. Techert, M. Lundberg, P. Wernet, K. Gaffney, M. Odelius, and A. Föhlisch, *J. Phys. Chem. Lett.* **9**, 3538 (2018).
- ²⁴ K. Hong, H. Cho, R.W. Schoenlein, T.K. Kim, and N. Huse, *Acc. Chem. Res.* **48**, 2957 (2015).
- ²⁵ S.E. Canton, K.S. Kjær, G. Vankó, T.B. van Driel, S. Adachi, A. Bordage, C. Bressler, P.

- Chabera, M. Christensen, A.O. Dohn, A. Galler, W. Gawelda, D. Gosztola, K. Haldrup, T. Harlang, Y. Liu, K.B. Møller, Z. Németh, S. Nozawa, M. Pápai, T. Sato, T. Sato, K. Suarez-Alcantara, T. Togashi, K. Tono, J. Uhlig, D.A. Vithanage, K. Wärnmark, M. Yabashi, J. Zhang, V. Sundström, and M.M. Nielsen, *Nat. Commun.* **6**, 6359 (2015).
- ²⁶ M. Izquierdo, M. Karolak, D. Prabhakaran, A.T. Boothroyd, A.O. Scherz, A. Lichtenstein, and S.L. Molodtsov, *Commun. Phys.* **2**, 8 (2019).
- ²⁷ N.A. Miller, A. Deb, R. Alonso-Mori, J.M. Glowina, L.M. Kiefer, A. Konar, L.B. Michocki, M. Sikorski, D.L. Sofferan, S. Song, M.J. Toda, T.E. Wiley, D. Zhu, P.M. Kozlowski, K.J. Kubarych, J.E. Penner-Hahn, and R.J. Sension, *J. Phys. Chem. A* **122**, 4963 (2018).
- ²⁸ N.A. Miller, A. Deb, R. Alonso-Mori, B.D. Garabato, J.M. Glowina, L.M. Kiefer, J. Koralek, M. Sikorski, K.G. Spears, T.E. Wiley, D. Zhu, P.M. Kozlowski, K.J. Kubarych, J.E. Penner-Hahn, and R.J. Sension, *J. Am. Chem. Soc.* **139**, 1894 (2017).
- ²⁹ K. Zhang, M.F. Lin, E.S. Ryland, M.A. Verkamp, K. Benke, F.M.F. De Groot, G.S. Girolami, and J. Vura-Weis, *J. Phys. Chem. Lett.* **7**, 3383 (2016).
- ³⁰ K. Zhang, G.S. Girolami, and J. Vura-Weis, *J. Synchrotron Radiat.* **25**, 1600 (2018).
- ³¹ E.S. Ryland, M.-F. Lin, M.A. Verkamp, K. Zhang, K. Benke, M. Carlson, and J. Vura-Weis, *J. Am. Chem. Soc.* **140**, 4691 (2018).
- ³² F. de Groot and A. Kotani, *Core Level Spectroscopy of Solids* (CRC Press, 2008).
- ³³ K. Zhang, R. Ash, G.S. Girolami, and J. Vura-Weis, ChemRxiv 10.26434/chemrxiv.8259011.v1 (2019).
- ³⁴ E.S. Ryland, K. Zhang, and J. Vura-Weis, *J. Phys. Chem. A* **123**, 5214 (2019).
- ³⁵ C.-M. Jiang, L.R. Baker, J.M. Lucas, J. Vura-Weis, A.P. Alivisatos, and S.R. Leone, *J. Phys. Chem. C* **118**, 22774 (2014).
- ³⁶ J. Vura-Weis, C.M. Jiang, C. Liu, H. Gao, J.M. Lucas, F.M.F. De Groot, P. Yang, a. P. Alivisatos, and S.R. Leone, *J. Phys. Chem. Lett.* **4**, 3667 (2013).
- ³⁷ S. Biswas, J. Husek, S. Londo, E.A. Fugate, and L.R. Baker, *Phys. Chem. Chem. Phys.* **20**, 24545 (2018).
- ³⁸ L.R. Baker, C.-M. Jiang, S.T. Kelly, J.M. Lucas, J. Vura-Weis, M.K. Gilles, A.P. Alivisatos, and S.R. Leone, *Nano Lett.* **14**, 5883 (2014).
- ³⁹ L.M. Carneiro, S.K. Cushing, C. Liu, Y. Su, P. Yang, A.P. Alivisatos, and S.R. Leone, *Nat. Mater.* **16**, 819 (2017).
- ⁴⁰ J.R. Sutherland, E.L. Christensen, N.D. Powers, S.E. Rhyndard, J.C. Painter, and J. Peatross, *Opt. Express* **12**, 4430 (2004).
- ⁴¹ R. Santra and A. Gordon, *Phys. Rev. Lett.* **96**, 073906 (2006).
- ⁴² J. Vura-Weis, C.-M. Jiang, C. Liu, H. Gao, J.M. Lucas, F.M.F. de Groot, P. Yang, A.P. Alivisatos, and S.R. Leone, *J. Phys. Chem. Lett.* **4**, 3667 (2013).

- ⁴³ M. Kubin, M. Guo, T. Kroll, H. Löchel, E. Källman, M.L. Baker, R. Mitzner, S. Gul, J. Kern, A. Föhlisch, A. Erko, U. Bergmann, V. Yachandra, J. Yano, M. Lundberg, and P. Wernet, *Chem. Sci.* **9**, 6813 (2018).
- ⁴⁴ H. Cho, M.L. Strader, K. Hong, L. Jamula, E.M. Gullikson, T.K. Kim, F.M.F. De Groot, J.K. McCusker, R.W. Schoenlein, and N. Huse, *Faraday Discuss.* **157**, 463 (2012).
- ⁴⁵ M.-F. Lin, M.A. Verkamp, J. Leveillee, E.S. Ryland, K. Benke, K. Zhang, C. Weninger, X. Shen, R. Li, D. Fritz, U. Bergmann, X. Wang, A. Schleife, and J. Vura-Weis, *J. Phys. Chem. C* **121**, 27886 (2017).
- ⁴⁶ P.L. Gentili, L. Bussotti, R. Righini, A. Beni, L. Bogani, and A. Dei, *Chem. Phys.* **314**, 9 (2005).
- ⁴⁷ E.A. Juban, A.L. Smeigh, J.E. Monat, and J.K. McCusker, *Coord. Chem. Rev.* **250**, 1783 (2006).
- ⁴⁸ E.A. Juban and J.K. McCusker, *J. Am. Chem. Soc.* **127**, 6857 (2005).
- ⁴⁹ E.M.S. Maçôas, S. Mustalahti, P. Myllyperkiö, H. Kunttu, and M. Pettersson, *J. Phys. Chem. A* **119**, 2727 (2015).
- ⁵⁰ E.M.S. Maçôas, R. Kananavicius, P. Myllyperkiö, M. Pettersson, and H. Kunttu, *J. Am. Chem. Soc.* **129**, 8934 (2007).
- ⁵¹ L.S. Forster, *Coord. Chem. Rev.* **227**, 59 (2002).
- ⁵² D.M. Adams, B. Li, J.D. Simon, and D.N. Hendrickson, *Angew. Chemie Int. Ed.* **34**, 1481 (1995).
- ⁵³ E. Evangelio, C. Rodriguez-Blanco, Y. Coppel, D.N. Hendrickson, J.P. Sutter, J. Campo, and D. Ruiz-Molina, *Solid State Sci.* **11**, 793 (2009).
- ⁵⁴ E. Evangelio and D. Ruiz-Molina, *Comptes Rendus Chim.* **11**, 1137 (2008).
- ⁵⁵ C. Boskovic, in *Spin-Crossover Mater. Prop. Appl.*, edited by M. Halcrow, 1st ed. (John Wiley & Sons, Ltd., West Sussex, 2013), pp. 203–224.
- ⁵⁶ O.-S. Jung, D.H. Jo, Y.-A. Lee, B.J. Conklin, and C.G. Pierpont, *Inorg. Chem.* **36**, 19 (1997).
- ⁵⁷ A. Hauser, *Coord. Chem. Rev.* **111**, 275 (1991).
- ⁵⁸ J.D. Koralek, J.B. Kim, P. Brůža, C.B. Curry, Z. Chen, H.A. Bechtel, A.A. Cordones, P. Sperling, S. Toleikis, J.F. Kern, S.P. Moeller, S.H. Glenzer, and D.P. DePonte, *Nat. Commun.* **9**, 1353 (2018).
- ⁵⁹ M. Ekimova, W. Quevedo, M. Faubel, P. Wernet, and E.T.J. Nibbering, *Struct. Dyn.* **2**, 054301 (2015).